Modelling an Advanced Gas-Cooled Reactor (AGR) Core using ABAQUS

Derek K. L. Tsang[1], Barry J. Marsden[1] and Graham B. Heys[2]

[1]Nuclear Graphite Research Group, School of MACE, The University of Manchester, Manchester UK, M13 9PL

[2] Office for Nuclear Regulation, an Agency of the Health and Safety Executive, Merseyside UK, L20 7HS

Abstract: The AGR graphite core not only acts as a moderator, but also as a major structural component. It is formed from a multi-layered array of loosely connected graphite bricks located together by a system of graphite keys and keyways. There are two different types of graphite bricks, namely fuel bricks and interstitial bricks. The core has 12 layers of brick forming about 320 fuel channels. Component dimensional changes due to fast neutron damage results in the generation of internal stresses and the distortion of the individual graphite components. This leads to change to the geometrical configuration of the reactor core as a whole. As part of the operational safety case, prediction of the core behaviour is required for both normal operation and fault conditions. An irradiated graphite material UMAT subroutine models the through life behaviour of the core components, but the whole core structure is so large with many interactions that an ABAQUS model would normally put excessive demands on computational resources. However this difficulty has been overcome by making use of superelements and parallel programming.

The code Manchester AGR Core Modelling (MANACM) contains a collection of three-dimensional user superelements and a UEL subroutine. The UEL is written in FORTRAN 90 and to be executed fully within ABAQUS. Each graphite component is represented by a superelement which includes contact elements to model the interactions. ABAQUS python script has been used to create an output database file from MANACM's results at the end of simulation. The modelling approach used by the MANACM is described in this paper.

Keywords: Constitutive Model, Output Database, Elasticity.

1. Introduction

A reactor core in the Advanced Gas-cooled Reactor (AGR) has graphite structure used as moderator. The graphite core is a multi-layered arrangement of discrete graphite bricks that are loosely connected to each other using a system of keys located in keyways. There are two types of bricks, of different size and geometry, namely fuel bricks and interstitial bricks (see Figure 1). The fuel bricks are hollow in shape and are stacked in layers to form fuel channels. The interstitial bricks are also hollow in shape and are stacked to form control rod and other utility channels. There are 12 layers of graphite brick in a typical AGR graphite core and each layer has 320 fuel

channels. The stacked bricks in each channel are keyed to the bricks in the adjacent channels using a combination of loose and integral keys located in keyways.

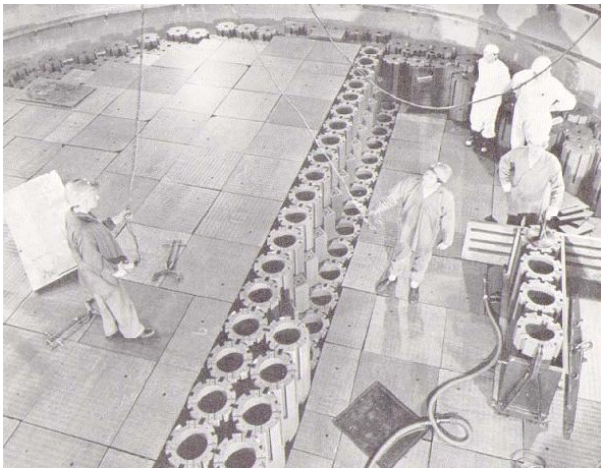

Figure 1. AGR core during assembly

The ageing deformation of the AGR graphite core structure is mainly due to physical changes arising from irradiation induced graphite dimensional change. These dimensional changes lead to distortion of the individual graphite components, which in turn result in changes to the geometrical configuration of the whole core. Irradiation induced dimensional change is a function of fast neutron fluence, irradiation temperature and radiolytic weight loss, therefore component deformation is complex and depends on position in the core. Moreover, cracks have been observed in a small percentage of fuel bricks which occur due to the build-up of internal stresses which arise from through-brick dimensional change rate.

The fundamental safety requirements of the graphite cores are to allow free movement of control rods and fuel, and to direct the flow of coolant gas to ensure adequate cooling of the fuel and the core structure, both in normal and fault/hazard conditions. Consequently safety cases demonstrating the tolerability of core safety functions to geometrical changes and cracked bricks are required.

Finite element methods have been used to model the reactor core components. One major advantage of finite element analysis is that it can provide detailed displacement and stress solutions for individual components. Also the effects of irradiation and the thermal expansion can be included in the analyses. An irradiated graphite material UMAT subroutine can be used to model the through life behaviour of the core components. However it is impossible to model the whole core using the conventional finite element method. The whole core structures are so large and complex that a conventional finite element model of the complete whole core structure would put excessive demands on available computational resources.

Manchester AGR Core Modelling (MANACM) is a collection of superelement models and a user element subroutine (UEL) to model the graphite components in reactor cores under irradiation and radiolytic conditions. Each graphite component has been represented by a superelement. The dimensional change and irradiation creep have been considered within the MANACM. ABAQUS python script has been used to create an output database file from MANACM's results at the end of simulation. The modelling approach used by the MANACM is described in this paper.

2. Irradiated graphite behaviour

There are two processes in nuclear reactors which modify the graphite properties significantly. The first process is the creation of lattice defects by the energetic radiation, principally the neutrons. The neutrons emitted in the fission process in the nuclear fuel of a thermal reactor lose their excess energy in collisions with the nuclei of the moderator atoms. A primary atomic displacement produced by a neutron-nuclei collision with a carbon atom produces a cascade of further displacements. Detailed calculations have been performed by (Thompson, 1965) and (Simmons, 1965). The calculations have indicated that 200-1000 atoms are displaced by the most energetic collisions, spread out over a large volume, such that it is a good approximation to consider that the displacements occur at random. During irradiation, crystal interstitials and vacancies are formed when fast neutrons displace carbon atoms from their lattice positions. These point defects can recombine to form a vacancy or interstitial loop. The rate and extent to which the recombination takes place is dependent on the irradiation temperature. Measurements of the crystal lattice parameters using X-rays showed that the interlayer spacing increases while the atomic spacing in the layer decreases under irradiation. Direct transmission electron microscopy by (Reynolds, 1965) showed that the crystal growth is due to the formation and growth of interstitial dislocation loops. The large basal plane contractions can be explained by the collapse of linear vacancy groups, the two-dimensional analogue of the vacancy loop. In short, neutrons bombardment of graphite initially creates point defects, which, depending on the irradiation temperature lead to more complex defects with increasing irradiation fluence. The lattice defects lead to the changes in the properties of the graphite.

The second process is radiolytic oxidation. Under fault conditions graphite oxidation by thermal reaction can predominate in the high temperature gas-cooled reactor. However, thermal oxidation is insignificant in the lower temperature carbon-dioxide cooled graphite moderators. Radiolytic oxidation occurs when carbon-dioxide is decomposed by ionising radiation to give reactive oxidising species. The rate of graphite oxidation is proportional to the rate of production of the oxidising species, which is itself a function of radiation intensity and gas pressure (but is substantially independent of temperature). Reviews which summarise the relevant information on oxidation of graphite due to radiolytic activation of carbon dioxide and the combination of the effects of oxidation with those of irradiation damage to predict the operational life of the graphite moderator can be found in (Best, 1985) and (Kelly, 1985).

In this section, changes in the structural, mechanical and thermal properties of graphite due to fast neutron irradiation and radiolytic oxidation are given. Property variations are given as a function of fast neutron fluence, temperature and fractional weight loss.

2.1 Young's modulus

Following irradiation the stress-strain relationship becomes more linear and the permanent set is decreased. Experiments to determine the elastic response of irradiated graphite have tended to concentrate on the dynamic Young's modulus as the basis of measurement. At low irradiation fluence levels there is a rapid increase in modulus followed by a constant state. At higher fluence levels the Young's modulus shows a gradual increase to a peak followed by a fall (see Figure 2).

There are two distinct mechanisms involved in these changes, firstly due to changes in the elastic constants of the graphite crystals and secondly due to changes in the bulk structure of the graphite. The first of these which is responsible for the initial rise in Young's modulus, is attributed to the pinning of the crystal basal planes and this effect soon saturates. The second, is attributed to differential straining of the polycrystalline micro-structure due to crystal growth and porosity closure leading to an increase in modulus. However, at even large crystal strains micro-cracks are generated which eventually leads to the reduction of the modulus and loss of strength.

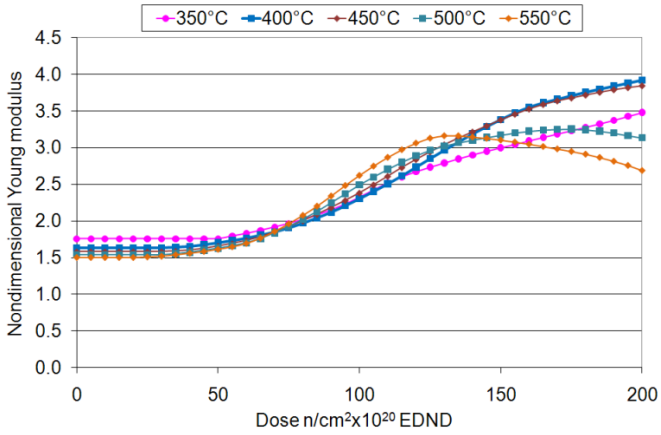

Figure 2: Irradiated Young's modulus against fluence (dose) at different temperature

2.2 Irradiation creep

The fact that graphite undergoes irradiation induced creep is important because, as graphite moderator blocks in a nuclear reactor are subjected to significant temperature and irradiation fluence gradients, and irradiation induced dimensional changes in graphite are both temperature and fluence dependent, these lead to self-induced stresses to be imposed on the blocks. These stresses would build up to levels exceeding the fracture strength of graphite in many cases if these stresses were not relieved by irradiation creep.

The creep coefficient is considered to be equal in tension and compression for a given graphite. Irradiation creep strain is defined as the difference in dimensions between a stressed sample and a sample with the same properties as the stressed sample irradiated unstressed. It has been

postulated that the irradiation creep in graphite is due to slip in the basal plane activated by the neutron irradiation and not by internal stress. The creep rate is considered to be proportional to stress and practically independent of temperature in the range 300-650℃.

Irradiation creep can be characterised by a transient stage followed by a linear stage. The magnitude of both primary transient creep and secondary creep was found to be proportional to stress and inversely proportional to the unirradiated modulus of elasticity.

2.3 Coefficient of thermal expansion

Fast neutron irradiation fluence modifies the coefficient of linear thermal expansion (CTE). This change is a function of the irradiation fluence, irradiation temperature and actual temperature. However, graphite CTE does not appear to be markedly affected by radiolytic oxidation. Typical irradiated CTE profiles at different temperatures are shown in Figure 3.

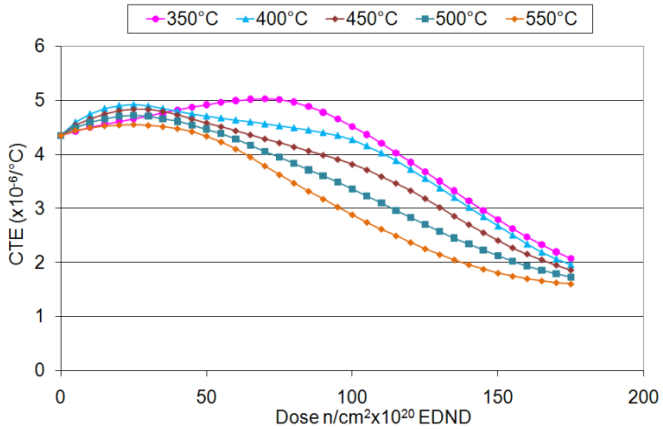

Figure 3. Irradiated CTE against fluence (dose) at different temperature

2.4 Dimensional change

Radiation damage by fast neutron fluence causes crystal growth in the c-axis direction and shrinkage in the a-axis direction. The effect of these irradiation induced crystal changes on the dimensional changes in isotropic moderator graphite has been reviewed by (Neighbour, 2000). Neutron irradiation of polygranular reactor graphites results in initial bulk shrinkage at low neutron fluence, leading eventually to a net expansion of the graphite with increasing fluence. Above irradiation temperature of 300℃, the initial effect of neutron irradiation on the microstructure of the graphite is closure of small pores and cracks as a result of c-axis expansion and contraction of the crystallites in the a-axis causing the initial bulk shrinkage of the graphite. The reversal of shrinkage, called ‘turnaround’, is believed to begin when the shrinkage cracks are unable to accommodate new irradiation-induced crystallite growth. At higher irradiation temperatures, turnaround occurs at lower neutron fluence. This is attributed to a reduction in the extent of accommodation available for irradiation-induced c-axis expansion as a result of closure

of Mrozowski cracks by thermal expansion. With further crystallite growth after turnaround, internal stresses develop to the point where new micro-cracks and pores begin to appear. Typical dimensional change profiles at different temperatures are shown in Figure 4.

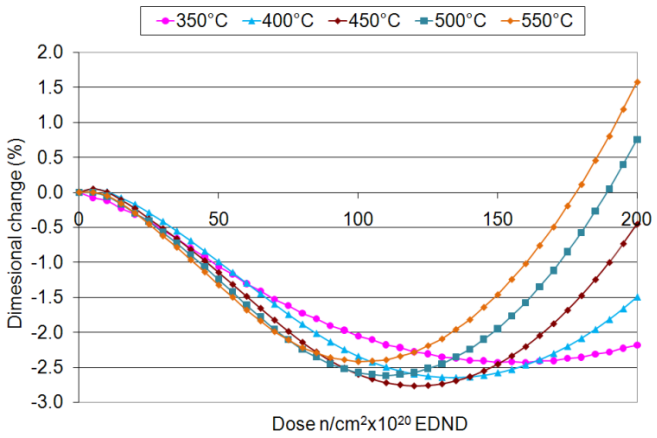

Figure 4. Dimensional change against fluence (dose) at different temperature

3. Superelement technique

In the early 1960s, a superelement technique was used by aerospace engineers to break down the structure of an airplane into simpler first-level substructures for enhancing the computational efficiency. If repeated parts appear in a structure, it is appropriate to apply the superelement technique. There are several advantages in using the superelement technique comparing with conventional finite element method:

- Stiffness matrices are small in superelement analyses. Subsequent to the creation of superelement, only the retained degrees of freedom and the associated superelement stiffness matrix are used in the analyses.
- Efficiency is improved when the same superelement is used multiple times. The stiffness calculation is done only once in each time step. However, the superelement itself can be used many times, resulting in a significant saving in computational effort.
- Superelement provides a systematic approach to complex analyses. Each graphite components can be represented by a superelement. Hence the amount of pre-processing time can be reduced significantly.

The substructure functionality (similar to superelement technique) is available in ABAQUS. However, the substructure function in ABAQUS is only for a linear problem and it isn't suitable for a nonlinear problem as in nuclear graphite analysis.

The frontal scheme has proved to be very efficient for solving positive definite matrix equations. At the time, there was a need to solve finite element problems that were too large for the system matrix and the matrix factors to be held in main memory, so that existing direct methods could not be used. The frontal method was therefore designed to be a robust direct method that required only a small amount of main memory. Today computers and their memories are much larger but so too are the problems that computational engineers wish to solve. Thus methods that require only limited main memory remain attractive. The MANACM applies the frontal method during element assembly: eliminates fully summed stiffness matrix but keeps stiffness matrix from retained nodes. Consequently the memory usage has been minimized.

4. Constitutive equations

The MANACM is designed for transversely isotropic material. The total strain within irradiated graphite $\boldsymbol{\varepsilon}_{\text{total}}$ is a sum of five different strains. They are the elastic strain $\boldsymbol{\varepsilon}_e$, the primary creep strain $\boldsymbol{\varepsilon}_{pc}$, the secondary creep strain $\boldsymbol{\varepsilon}_{sc}$, the dimensional change strain $\boldsymbol{\varepsilon}_{dc}$ and the thermal strain $\boldsymbol{\varepsilon}_{th}$, i.e.

$$\boldsymbol{\varepsilon}_{\text{total}} = \boldsymbol{\varepsilon}_e + \boldsymbol{\varepsilon}_{pc} + \boldsymbol{\varepsilon}_{sc} + \boldsymbol{\varepsilon}_{dc} + \boldsymbol{\varepsilon}_{th}. \tag{1}$$

The elastic strain $\boldsymbol{\varepsilon}_e$ is related to the stress $\boldsymbol{\sigma}$ by means of the usual Hooke's law of linear elasticity, i.e.

$$\boldsymbol{\sigma} = \mathbf{D}\boldsymbol{\varepsilon}_e. \tag{2}$$

The primary creep strain $\boldsymbol{\varepsilon}_{pc}$ is defined as

$$\frac{d\boldsymbol{\varepsilon}_{pc}}{d\gamma} = 4\varphi\left(\mathbf{D}_{pc}\boldsymbol{\sigma} - \boldsymbol{\varepsilon}_{pc}\right), \tag{3}$$

where γ is the radiation fluence, $\varphi = \varphi(T)$ is a temperature dependent parameter and $\mathbf{D}_{pc}$ is the primary creep material matrix. The secondary creep strain $\boldsymbol{\varepsilon}_{sc}$ is defined as

$$\frac{d\boldsymbol{\varepsilon}_{sc}}{d\gamma} = \xi\mathbf{D}_{sc}\boldsymbol{\sigma}, \tag{4}$$

where $\xi = \xi(T)$ is a temperature dependent parameter and $\mathbf{D}_{sc}$ is the secondary creep material matrix.

For a given temperature, the unrestrained dimensional change rate subject to irradiation γ and weight loss ϕ is given by

$$\frac{d\boldsymbol{\varepsilon}_{dc}}{d\gamma} = \mathbf{h}(\gamma, \phi). \tag{5}$$

The thermal strain is defined as

$$\boldsymbol{\varepsilon}_{th} = \boldsymbol{\alpha}_{(T_{ref}-T)}\left(T - T_{ref}\right), \tag{6}$$

where $\boldsymbol{\alpha}_{(T_{ref}-T)}$ is the mean coefficient of thermal expansion between a reference temperature T_{ref} ℃ and T ℃.

4.1 Numerical technique

It is desirable to use an implicit time scheme for a set of stiff differential equations. Consider a differential equation in the form

$$\frac{dy}{dt} = f\left(y,t\right). \tag{7}$$

A first order approximation for Equation (7) is

$$\Delta y = \Delta t\, f^{n+1}, \tag{8}$$

where $f^{n+1} = f\left(y^{n+1}, t^{n+1}\right)$. A second order approximation for Equation (7) is

$$\Delta y = \Delta t\left(\frac{f^{n+1} + f^{n}}{2}\right), \tag{9}$$

where $f^{n} = f\left(y^{n}, t^{n}\right)$. The first order approximation always gives stable numerical results, however, the solution only gives first order accuracy. The second order approximation gives better numerical results but it may produce an unstable solution for strong stiffness equation.

It is more convenient to rewrite Δy as

$$\Delta y = \Delta t\left(\beta_1 f^{n+1} + \beta_2 f^{n}\right), \tag{10}$$

when $\beta_1 = 1$ and $\beta_2 = 0$, Equation (10) gives the first order approximation and when $\beta_1 = \beta_2 = \frac{1}{2}$ it gives the second order approximation. This different order of approximation can be used for different strains and their orders are chosen according to their numerical behaviour.

The total change in strain (1) can be written as

$$\Delta\boldsymbol{\varepsilon}_{e} + \Delta\boldsymbol{\varepsilon}_{pc} + \Delta\boldsymbol{\varepsilon}_{sc} + \Delta\boldsymbol{\varepsilon}_{dc} + \Delta\boldsymbol{\varepsilon}_{th} - \Delta\boldsymbol{\varepsilon}_{\text{total}} = 0. \tag{11}$$

The change in thermal strain from Equation (6) can be written as

$$\Delta\boldsymbol{\varepsilon}_{th} = \Delta\boldsymbol{\alpha}_{(20-120)}\left(T - T_{ref}\right) + \boldsymbol{\alpha}_i \Delta T\,, \tag{12}$$

where $\boldsymbol{\alpha}_i$ is the instantaneous coefficient of thermal expansion. The change in dimensional change from Equation (5) can be written as:

$$\Delta\boldsymbol{\varepsilon}_{dc} = \Delta\gamma\left(\mathbf{h}\right). \tag{13}$$

Using Equations (2) and (10), the change in primary creep strain can be written as

$$\begin{aligned} -4\beta_1\varphi\Delta\gamma\mathbf{D}_{pc}^{n+1}\mathbf{D}^{n+1}\Delta\boldsymbol{\varepsilon}_e + \left(1+4\beta_1\varphi\Delta\gamma\right)\Delta\boldsymbol{\varepsilon}_{pc} \\ -4\varphi\Delta\gamma\left[\left(\beta_1\mathbf{D}_{pc}^{n+1}\mathbf{D}^{n+1} + \beta_2\mathbf{D}_{pc}^{n}\mathbf{D}^{n}\right)\boldsymbol{\varepsilon}_e^n - \left(\beta_1+\beta_2\right)\boldsymbol{\varepsilon}_{pc}^n\right] = 0 \end{aligned} \tag{14}$$

and the change in secondary creep strain can be written as

$$-\beta_1\xi\Delta\gamma\mathbf{D}_{sc}^{n+1}\mathbf{D}^{n+1}\Delta\boldsymbol{\varepsilon}_e + \Delta\boldsymbol{\varepsilon}_{sc} - \xi\Delta\gamma\left(\beta_1\mathbf{D}_{sc}^{n+1}\mathbf{D}^{n+1} + \beta_2\mathbf{D}_{sc}^{n}\mathbf{D}^{n}\right)\boldsymbol{\varepsilon}_e^n = 0 \tag{15}$$

Equations (11)-(15) are a system of equations which define all the strains within irradiated graphite. The change in thermal strain and dimensional change strain can be calculated explicitly. Hence a system of equations can be formed from Equations (11), (14) and (15), with unknowns $\Delta\boldsymbol{\varepsilon}_e$, $\Delta\boldsymbol{\varepsilon}_{pc}$ and $\Delta\boldsymbol{\varepsilon}_{sc}$. Therefore the system of equation can be written as

$$\mathbf{W}\left(\mathbf{X}\right) = \mathbf{0}\,, \tag{16}$$

where $\mathbf{X} = \left(\Delta\boldsymbol{\varepsilon}_e, \Delta\boldsymbol{\varepsilon}_{pc}, \Delta\boldsymbol{\varepsilon}_{sc}\right)$. Equation (16) can be solved using Newton's method. The Jacobian matrix $\mathbf{J} = \dfrac{\partial\mathbf{W}}{\partial\mathbf{X}}$ for Equation (16) used in Newton's method can be found analytically as

$$\mathbf{J} = \begin{pmatrix} \mathbf{I} & \mathbf{I} & \mathbf{I} \\ \mathbf{H} & \chi\mathbf{I} & \mathbf{0} \\ \mathbf{G} & \mathbf{0} & \mathbf{I} \end{pmatrix}, \tag{17}$$

where $\chi = 1+4\beta_1\varphi\Delta\gamma$. The matrixes $\mathbf{H}$ and $\mathbf{G}$ are defined as $\mathbf{H} = -4\beta_1\varphi\Delta\gamma\mathbf{D}_{pc}\mathbf{D}$ and $\mathbf{G} = -\beta_1\xi\Delta\gamma\mathbf{D}_{sc}\mathbf{D}$, respectively. Also the matrix $\mathbf{I}$ is unit matrix.

The Jacobian matrix of the constitutive model $\partial\Delta\boldsymbol{\sigma}/\partial\Delta\boldsymbol{\varepsilon}_{\text{total}}$ is required. The Jacobian matrix of the constitutive model can be written as

$$\frac{\partial\Delta\boldsymbol{\sigma}}{\partial\Delta\boldsymbol{\varepsilon}_{\text{total}}} = \left(\mathbf{D}^{-1} + \frac{4\varphi\Delta\gamma}{1+4\varphi\Delta\gamma}\mathbf{D}_{pc} + \xi\Delta\gamma\mathbf{D}_{sc}\right)^{-1}. \tag{18}$$

5. Numerical examples

A layer of core structure of different array sizes have been analysed using MANACM. For an array of size $n \times n$, there are n^2 number of fuel bricks, $3(n-1)^2$ number of interstitial bricks and $6n(n-1)$ keys. An example of 3x3 array size is shown in Figure 5. The interaction between each component has been modelled using ABAQUS contract elements.

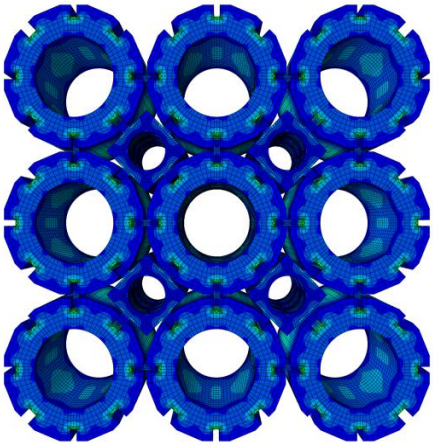

Figure 5. A layer of 3x3 array.

Figure 6 shows the total degree of freedom (DOF), including contract nodes, against different array sizes. The superelement model for a layer of 10x10 array has 151,144 nodes and total DOF is 380,856. However the corresponding normal ABAQUS model has over 4 million 3D elements and 20 million nodes. It is impossible to run the normal ABAQUS model due to the size.

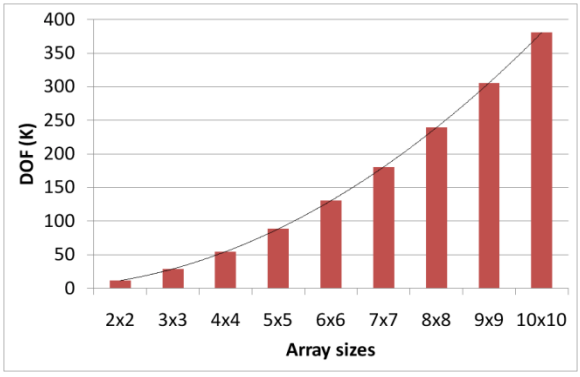

Figure 6. Total DOF against different array sizes using MANACM.

Figure 7 shows the memory usage against different array sizes. Three processors have been used in the analyses. Figure 8 shows corresponding computational time against array size. For an analysis of 2x2 array, the MANACN has needed 7GB of memory and 1.7 hours of computational time. However the corresponding ABAQUS model has required 17.7GB of memory and 3.3 hours of computational time. Although the total DOF has been increased by a factor of 33 from array size 2x2 to 10x10, the computational time and memory usage have been increased by only 20 times and 3 times, respectively.

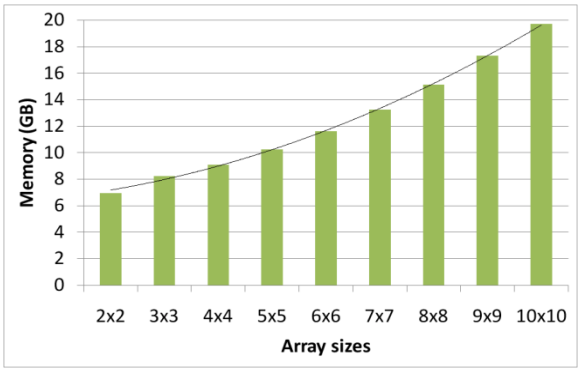

Figure 7. Total memory usage against different array sizes using MANACM.

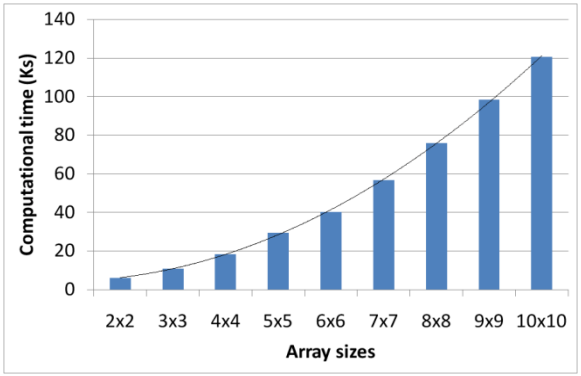

Figure 8. Computational time against different array sizes using MANACM.

Figure 9 shows the computational times against number of processors for a 6x6 array. The computational time has been decreased by using more processors. However the computational time using 8 processors is more than that for 7 processors. This is because ABAQUS has submitted more elements to a processor in 8 processors computation than in 7 processors computation. In 7 processors computation, one of seven processors has received 7 brick

superelements and 9 interstitial superelements. However in 8 processors computation, one of eight processors has received 7 brick superelements and 11 interstitial superelements. Consequently using 8 processors for the analysis has required more computational time than using 7 processors.

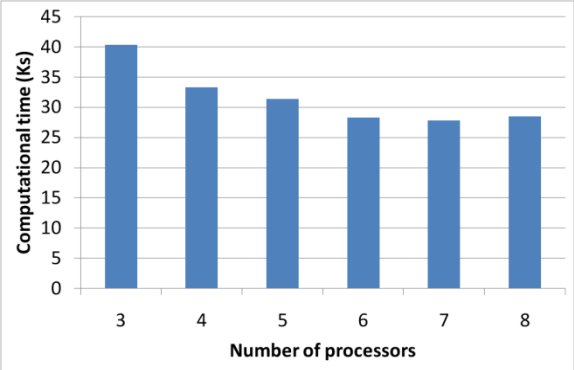

Figure 9. The computational times against number of processors for array of 6x6.

6. Conclusions

The code MANACM has been developed to model the graphite components in the AGR core. The code uses the superelement technique and parallel programming. The MANACM has been shown to be efficient to model the reactor core. The memory usage and computational times can be reduced significantly compared with normal finite element methods.

7. References

- Best, J.V., Stephen, W.J. and Wickham, A.J., "Radiolytic Graphite Oxidation", Progress in Nuclear Energy, 16, 127-178, 1985.
- Kelly, B.T., "The Radiolytic Corrosion of Advanced Gas-Cooled Reactor Graphite", Progress in Nuclear Energy, 16, 73-96, 1985.
- Neighbour, G.B., "Modelling of Dimensional Changes in Irradiated Nuclear Graphite", Journal of Physics D- Applied Physics, 33, 2966-2972, 2000.
- Reynolds, W.N. and Thrower, P.A., "Nucleation of Radiation Damage in Graphite", Philosophical Magazine, 12, 573-593, 1965.
- Simmons, J.H.W., Radiation Damage in Graphite, Pergamon, 1965.
- Thompson, M. W. and Wright, S.B., "A New Damage Function for Predicting the Effect of Reactor Irradiation on Graphite in Different Neutron Spectra", Journal of Nuclear Materials, 16, 146-154, 1965.

8. Acknowledgements

The authors would like to thank the Office for Nuclear Regulation for financial support of this project. The opinions expressed in this paper are those of the authors and do not necessarily represent those of the Office for Nuclear Regulation.